Article

Thermoelectric Performance of the MXenes MCO (M = Ti, Zr, or Hf)

Appala Naidu Gandi, Husam N. Alshareef, and Udo Schwingenschlögl

Chem. Mater., **Just Accepted Manuscript** • DOI: 10.1021/acs.chemmater.5b04257 • Publication Date (Web): 21 Feb 2016

Chemistry of Materials is published by the American Chemical Society. 1155 Sixteenth Street N.W., Washington, DC 20036

Thermoelectric Performance of the MXenes M_2CO_2 (M = Ti, Zr, or Hf)

Appala Naidu Gandi, Husam N. Alshareef, and Udo Schwingenschlögl*

King Abdullah University of Science and Technology (KAUST), Physical Science and Engineering Division (PSE), Thuwal 23955-6900, Saudi Arabia

E-mail: udo.schwingenschlogl@kaust.edu.sa

Abstract

We present the first report in which the thermoelectric properties of two-dimensional MXenes are calculated by considering both the electron and phonon transport. Specifically, we solve the transport equations of the electrons and phonons for three MXenes, M_2CO_2, where M = Ti, Zr, or Hf, in order to evaluate the effect of the metal M on the thermoelectric performance. The lattice contribution to the thermal conductivity, obtained from the phonon life times, is found to be lowest in Ti_2CO_2 and highest in Hf_2CO_2 in the temperature range from 300 K to 700 K. The highest figure of merit is predicted for Ti_2CO_2. The heavy mass of the electrons due to flat conduction bands results in a larger thermopower in the case of n-doping in these compounds.

*To whom correspondence should be addressed

Introduction

MXenes are two-dimensional crystalline materials obtained from the MAX phases $M_{n+1}AX_n$. Since there is a multitude of MAX phases and due to the possibility to saturate the transition metal (M) with functional groups, many MXenes can be fabricated, encompassing a broad range of compositions and hence a broad range of properties and potential applications.[1,2] The functional groups O, F, and OH result from the etching of the MAX phases. Experiments have addressed applications of MXenes in Li-ion batteries,[3] catalysis,[4] electrochemical capacitors,[5] and fuel cells.[6] Whether an MXene is a semiconductor (as required for thermoelectric usage) or not depends on the functional group and its orientation.[7] According to first principles calculations, Ti_2CO_2, Zr_2CO_2, Hf_2CO_2, Sc_2CF_2, $Sc_2C(OH)_2$, and Sc_2CO_2 are semiconductors.[8] Ti_2CO_2 has a narrow band gap of 0.17-0.44 eV,[9–11] thus being interesting for thermoelectric applications, and shows a high carrier mobility.[12] Zr_2CO_2 and Hf_2CO_2 share many properties with Ti_2CO_2 because of their structural and compositional similarity.[10]

First principles calculations predict high Seebeck coefficients (1100 μV/K and 2000 μV/K, respectively)[8] and power factors[10] for Ti_2CO_2 and $Sc_2C(OH)_2$ at 100 K. However, these electronic quantities are not sufficient to determine the thermoelectric efficiency, since the lattice contribution to the thermal conductivity also influences the figure of merit. Indeed, most of the heat conduction happens through phonons in semiconductors. To calculate the lattice contribution, we therefore solve the Boltzmann transport equation for phonons self-consistently and evaluate the phonon lifetimes. This allows us to provide a first comprehensive account of the thermoelectric performance of MXenes. In particular, we will study the role of the transition metal for the material properties.

Methodology

First principles calculations are performed using the Vienna Ab-initio Simulation Package.[13] Plane waves with energies up to 500 eV are employed in the expansion of the electronic wave functions, considering the C $2s^2$, $2p^2$ and O $2s^2$, $2p^4$ electrons as valence states. For Ti, Zr, and Hf twelve electrons are considered as valence states. We employ the generalised gradient approximation of the exchange-correlation potential in the Perdew-Burke-Ernzerhof flavour.[14] Brillouin zone integrations are performed using the tetrahedron method with Blöchl corrections.[15] The MXenes are constructed by connecting a 15 Å vacuum slab to an O-M-C-M-O slab along the c-direction. Increasing the thickness of the vacuum slab to 20 Å modifies the total energy by less than 1 meV. Γ-centered $24 \times 24 \times 1$ k-meshes are used for optimising the structures (hexagonal symmetry, P$\bar{3}$m1). Since spin-polarised calculations find vanishing magnetic moments, we present in the following the results of spin-degenerate calculations. We consider different locations of the ligands and confirm the lowest energy configuration reported in the literature,[9] for which we evaluate the thermoelectric properties.

We solve the semi-classical Boltzmann transport equation within the constant relaxation time approximation ($\tau = 10^{-14}$ s) for calculating the Seebeck coefficient, electrical conductivity, and electronic contribution to the thermal conductivity. While the relaxation time τ in general depends on the electronic wave vector, energy, and scattering mechanism, reliable results for the transport properties have been obtained within the constant relaxation time approximation for a variety of materials.[16–18] A rigid band approximation is used to simulate doping by shifting the chemical potential (BoltzTraP code[19]). For this purpose, the electronic band structure is calculated on a very fine $42 \times 42 \times 1$ k-mesh.

We follow the supercell based direct method to calculate the normal mode polarisation vectors and phonon frequencies within the harmonic approximation.[20] A $4 \times 4 \times 1$ supercell is chosen with a $3 \times 3 \times 1$ k-mesh for evaluating the forces and the method of Cochran and coworkers[21] is used for including long range dipole interactions to the dynamical matrix. The dielectric tensor and Born effective charges are evaluated using perturbation theory.[22] In

Table 1: Lattice constants and bond lengths obtained by structure relaxation.

	Ti_2CO_2	Zr_2CO_2	Hf_2CO_2
a (Å)	3.031	3.309	3.268
M–O (Å)	1.972	2.120	2.104
M–C (Å)	2.184	2.368	2.336
C–O (Å)	2.823	3.003	2.980

addition, we employ a finite difference scheme for evaluating the third order force constants,[23] where each atom up to fifth nearest neighbours is simultaneously displaced with a given atom (interaction distance up to 4.87 Å). Translational invariance conditions are imposed on the force constants.[24] The second and third order force constants are used for solving a linearised version of the Boltzmann transport equation for the phonons numerically by the ShengBTE code.[25,26] For this purpose, Brillouin zone integrations are carried out on a $36 \times 36 \times 1$ k-mesh, for which our convergence tests find a difference of less than 0.1% in the lattice thermal conductivity as compared to a $33 \times 33 \times 1$ k-mesh. The results for $3 \times 3 \times 1$ and $4 \times 4 \times 1$ supercells deviate by less than 1%. The volume dependent output of the ShengBTE code is scaled by assuming that the thickness equals the vertical distance between the top and bottom O planes.

At room temperature the thermal resistivity is dominated by three phonon Umklapp scattering events, whereas scattering events involving four or more phonons become relevant when the temperature exceeds half of the melting temperature.[27] Since molecular dynamics simulations predict that Ti_2CO_2 remains solid up to 823 K,[28] we limit our analysis to 700 K and consider three phonon scattering events. Hence, for higher temperatures the conductivity values obtained from our procedure constitute upper limits.

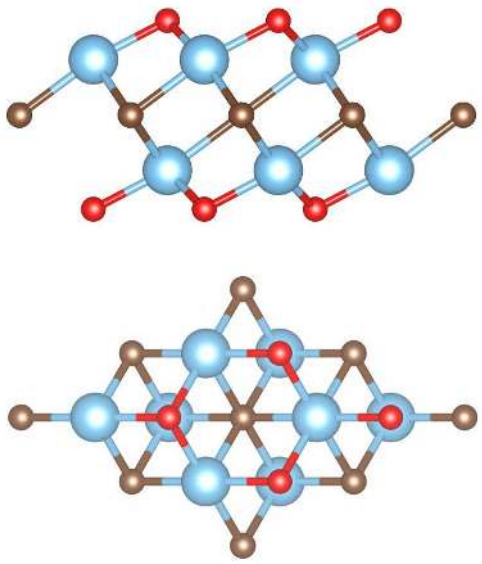

Figure 1: Side and top views of the crystal structure of the MXenes M_2CO_2 (M = Ti, Zr, or Hf). Blue, brown, and red spheres represent M, C, and O atoms.

Results and discussion

The lowest total energy is achieved when the O atoms in the top atomic layer of the MXene sandwich structure are located directly above the M atoms and the O atoms in the bottom atomic layer directly below them, see Figure 1. The corresponding equilibrium structure parameters are presented in Table 1. Because of their structural similarity, the three compounds under investigation have similar band structures, see Figure 2. The C 2p, O 2p, and M d states form the valence band edge, whereas the O 2p and M d states form the conduction band edge. We find in each case an indirect band gap with the valence band maximum at the Γ point and the conduction band minimum at the M point. Moreover, each compound shows a considerable asymmetry between the valence and conduction bands, thus between hole and electron doping. The band forming the conduction band edge is very flat, whereas that forming the valence band edge is dispersive (spreading over 3 eV). Thus, the effective mass of the electrons is much larger than that of the holes and consequently n-doping leads to a higher Seebeck coefficient than p-doping, as seen in Figures 3 and 4. While the main features of the band structures are similar, the three compounds are distinguished by their

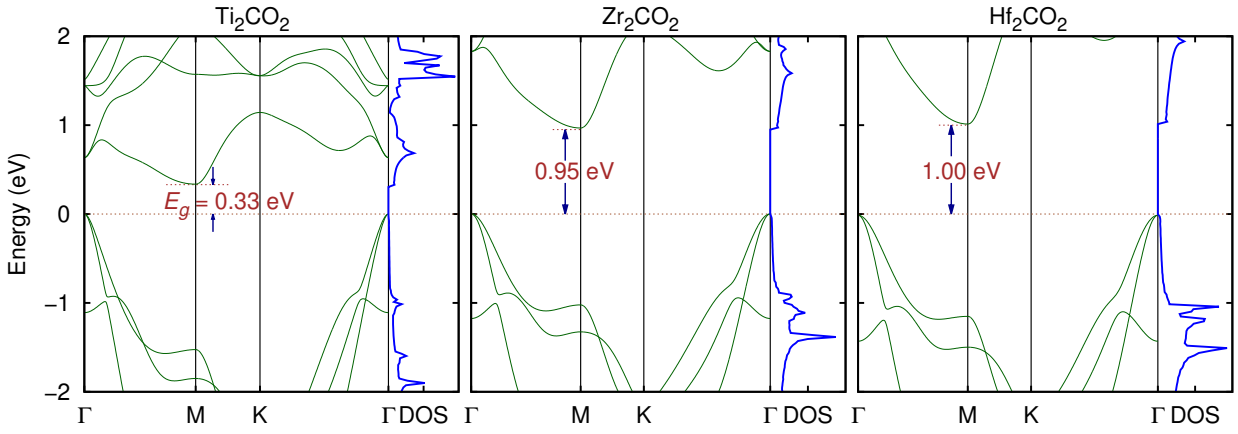

Figure 2: Electronic band structures and densities of states.

band gaps, which agree in size with previous results obtained by similar methodologies but are lower than those found by Heyd-Scuseria-Ernzerhof calculations.[8–11] Having the largest band gap, Hf_2CO_2 shows the highest Seebeck coefficient at a given temperature and carrier concentration. The electrical conductivity and electronic contribution to the thermal conductivity are also shown in Figures 3 and 4 as functions of the carrier concentration.

In narrow band gap semiconductors at high temperatures and low carrier concentrations the minority carriers reduce the Seebeck coefficient and increase the electrical conductivity.[29] As both holes and electrons carry heat, the overall thermal conductivity increases.[30] These effects can be seen prominently in Figures 3 and 4 in the case of Ti_2CO_2 because of its narrow band gap, whereas they are small for Zr_2CO_2 and Hf_2CO_2.

The high frequency dielectric tensors and Born effective charges reported in Table 2 are used along with the second order force constants to determine the harmonic phonon dispersion relations shown in Figure 5. For Ti_2CO_2 we obtain excellent agreement with Ref. 8. In each case, there are three low frequency optical branches in close proximity to the acoustic branches with significant group velocities, which can increase the scattering cross-section of the acoustic phonons.[31] Thus, the first six branches are significant for the heat conduction.

The calculated lattice contributions to the thermal conductivity are plotted in Figure 6, where the fitting curve uses the fact that the thermal conductivity is inversely proportional

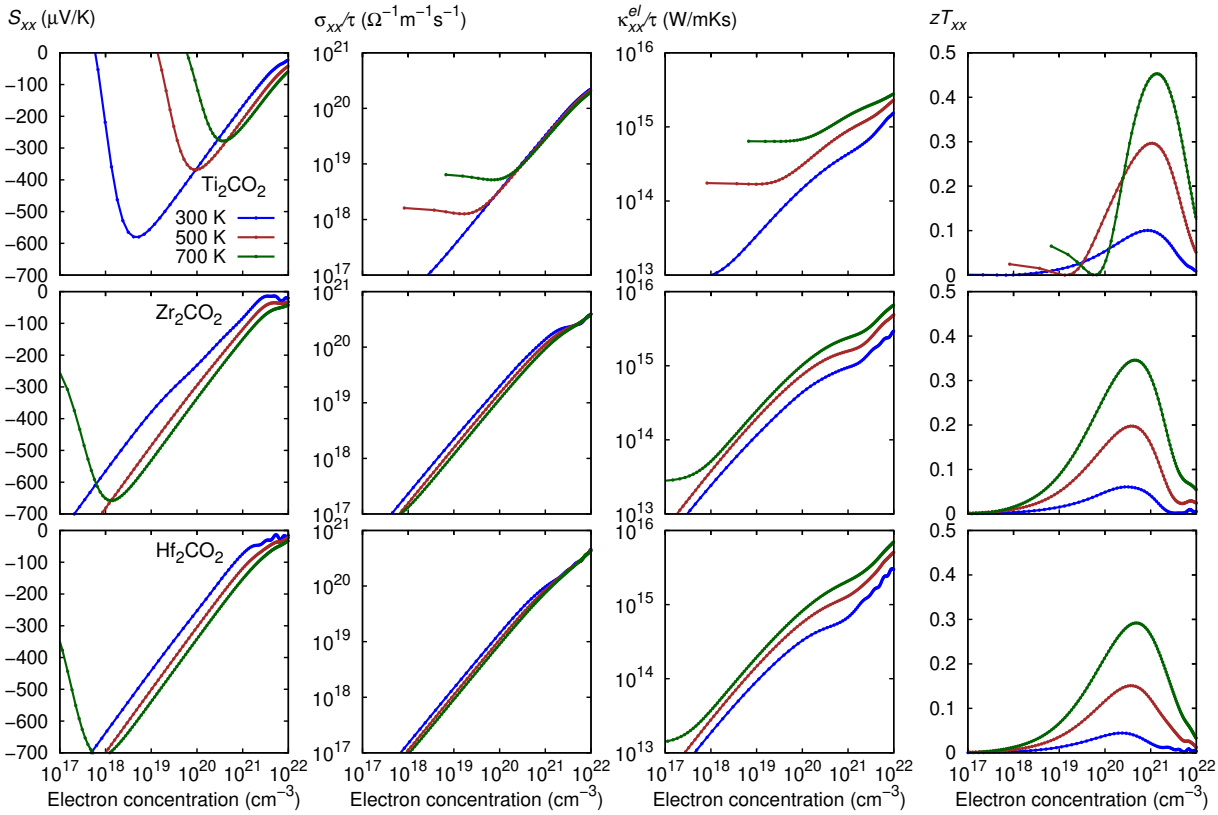

Figure 3: Transport coefficients as functions of the electron concentration.

to the temperature when limited by anharmonic scattering.[32] At room temperature more than 72% of the heat conduction happens through the first three phonon branches (acoustic branches), whereas the three low frequency optical branches account for 20%. We obtain excellent agreement with recently published room temperature values of 21.9 W/mK for Ti_2CO_2, 61.9 W/mK for Zr_2CO_2, and 86.3 W/mK for Hf_2CO_2.[33] Analysis of the phonon life times suggests that the phonon-phonon interaction is stronger in Ti_2CO_2 than in Zr_2CO_2 and Hf_2CO_2. While the group velocities are similar in the three compounds, the dispersion of the first six phonon branches is largest in Ti_2CO_2 and smallest in Hf_2CO_2 (see Figure 5). Presence of low frequency optical branches near the acoustic branches increases the likelihood of Umklapp scattering involving an acoustic mode and an optical mode.[32,34] Proximity of the fist six branches to each other and other optical branches is the reason for the increased scattering cross-section and lowest phonon life times in Ti_2CO_2.

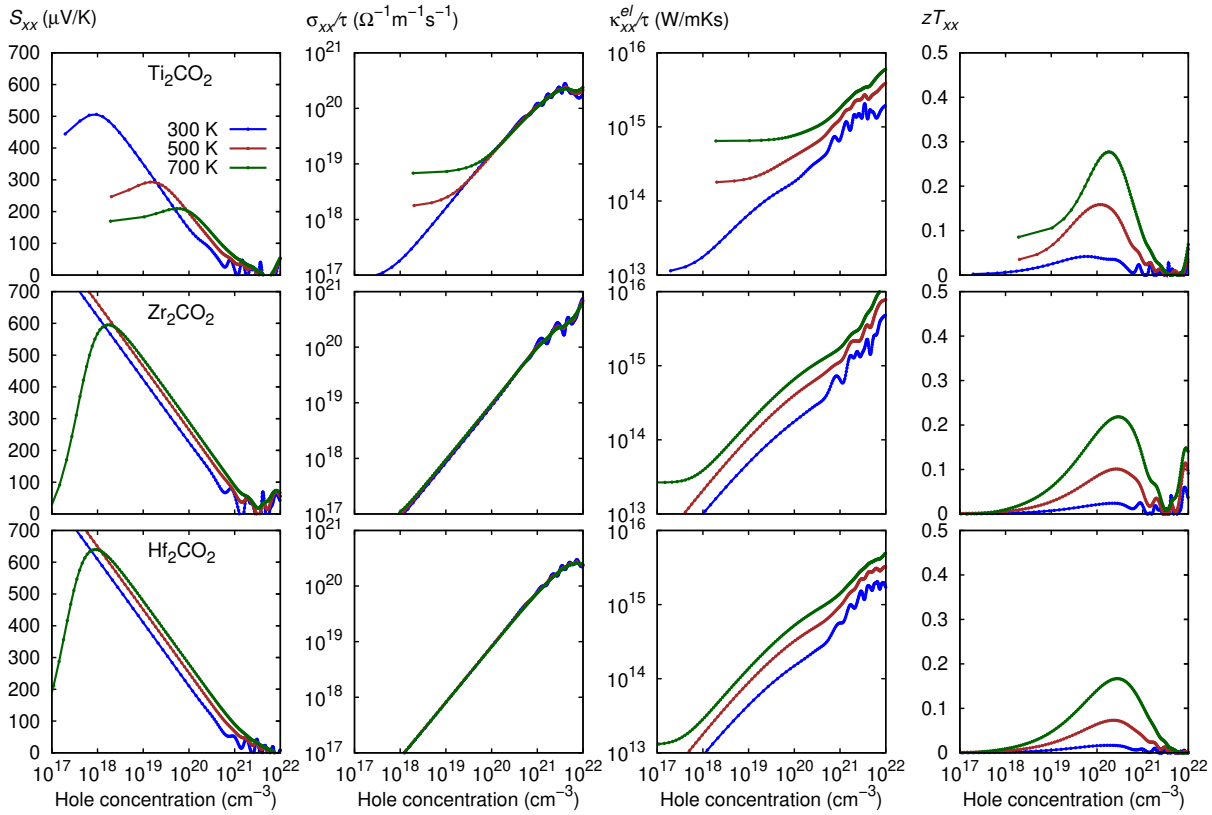

Figure 4: Transport coefficients as functions of the hole concentration.

According to Figures 3 and 4, the figure of merit is higher for n-doping than for p-doping, which is mainly due to the larger Seebeck coefficient. Ti_2CO_2 shows the best thermoelectric performance because of its lower lattice thermal conductivity as compared to Zr_2CO_2 and Hf_2CO_2. The peak values of the figure of merit and corresponding carrier concentrations are noted in Table 3. They correspond to a large area sample in which the heat conduction is diffusive. The mean free path of the phonons responsible for heat conduction is typically longer than that of the electrons in thermoelectric materials.[35] An improved thermoelectric performance thus is expected when the sample size is reduced below the maximal phonon mean free path, given in the rightmost column of Table 3, as the lattice contribution to the thermal conductivity is lowered (ballistic heat conduction) without adversely affecting the electrical conductivity.

Table 2: High frequency dielectric tensors and Born effective charges.

	Ti_2CO_2	Zr_2CO_2	Hf_2CO_2
$\varepsilon^{\infty}_{xx}$	32.04	17.46	15.37
Z^{*}_{xx}(M)	7.06	6.30	6.05
Z^{*}_{xx}(C)	−5.80	−5.24	−5.08
Z^{*}_{xx}(O)	−4.16	−3.68	−3.51

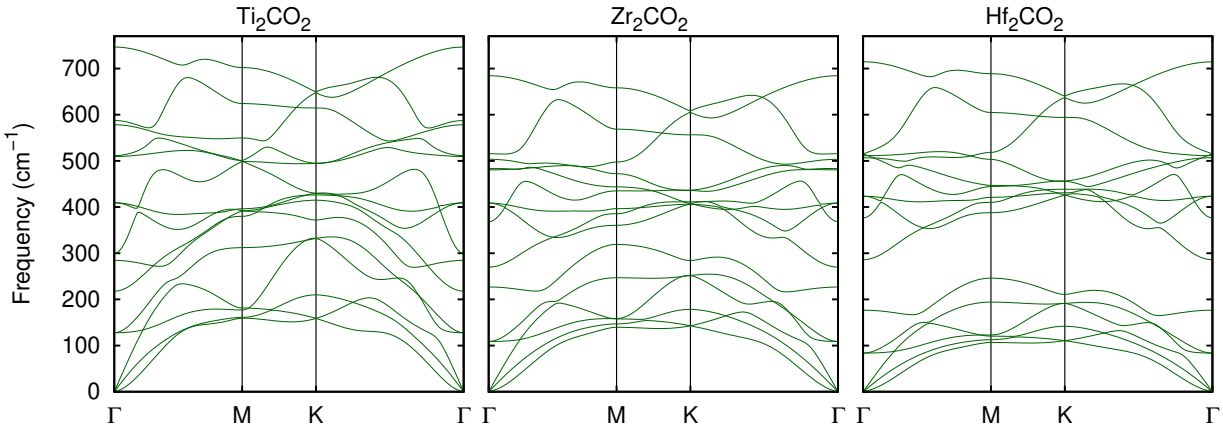

Figure 5: Harmonic phonon dispersion relations.

Conclusions

For the first time we have studied the thermoelectric properties of two-dimensional MXenes by considering both the electron and phonon transport. We have solved the Boltzmann transport equations for the electrons and phonons to quantify the electronic and lattice contributions to the figure of merit of the MXenes M_2CO_2 (M = Ti, Zr, or Hf). It turns out that the band gap grows with the mass of the M atom. Differences in the effective masses of the charge carriers explain why n-doping leads to larger Seebeck coefficients than p-doping. The lattice contribution to the thermal conductivity is smallest in Ti_2CO_2 as the acoustic phonon branches show the strongest dispersions. Below a carrier concentration of 1.4×10^{21} cm^{-3} electrons the figure of merit decreases drastically due to effects of the minority carriers. We have also determined the sample dimensions below which the heat transport becomes ballistic and the thermoelectric performance thus is enhanced.

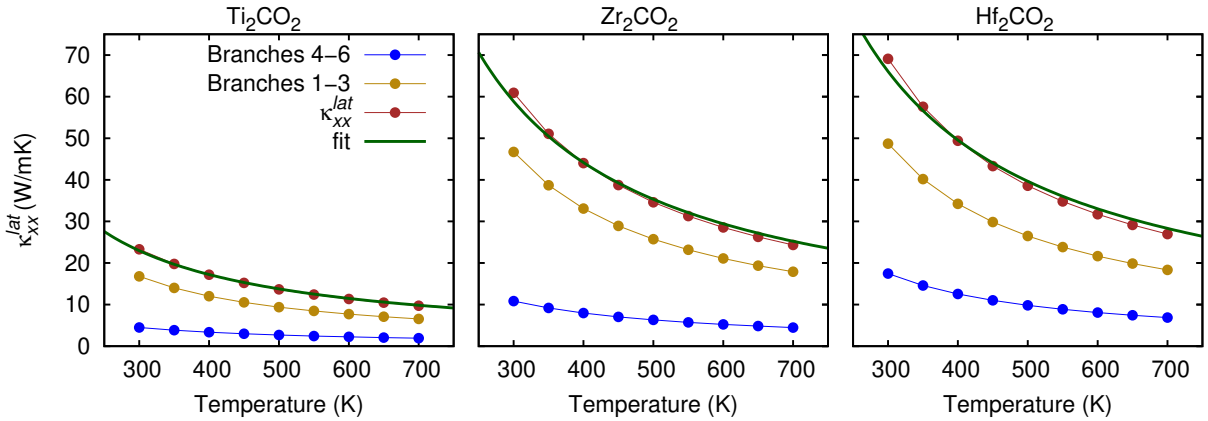

Figure 6: Lattice contributions to the thermal conductivity as functions of the temperature.

Table 3: Peak thermoelectric performances, corresponding carrier concentrations, and maximal phonon mean free paths (Λ_{max}) at 700 K.

	n-doping ($\times 10^{20}$cm^{-3})	zT	p-doping ($\times 10^{20}$cm^{-3})	zT	Λ_{max} (nm)
Ti_2CO_2	14.0	0.45	1.7	0.27	132
Zr_2CO_2	4.4	0.35	3.0	0.22	486
Hf_2CO_2	5.0	0.29	2.9	0.17	850

Acknowledgements

The research reported in this publication was supported by funding from King Abdullah University of Science and Technology (KAUST). Computational resources were provided by the Supercomputing Laboratory of KAUST.

Table of contents figure

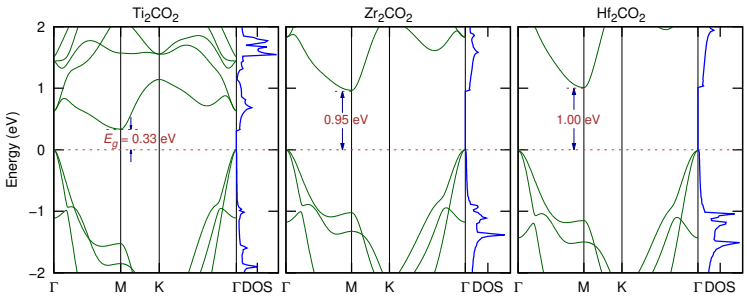

References

(1) Naguib, M.; Gogotsi, Y. Synthesis of Two-Dimensional Materials by Selective Extraction. *Acc. Chem. Res.* **2015**, *48*, 128–135

(2) Lei, J.-C.; Zhang, X,; Zhou, Z. Recent Advances in MXene: Preparation, Properties, and Applications. *Front. Phys.* **2015**, *10*, 276–286

(3) Mashtalir, O.; Naguib, M.; Mochalin, V. N.; Dall'Agnese, Y.; Heon, M.; Barsoum, M. W.; Gogotsi, Y. Intercalation and Delamination of Layered Carbides and Carbonitrides. *Nat. Commun.* **2013**, *4*, 1716

(4) Xie, X.; Chen, S.; Ding, W.; Nie, Y.; Wei, Z. An Extraordinarily Stable Catalyst: Pt NPs Supported on Two-Dimensional $Ti_3C_2X_2$ (X = OH, F) Nanosheets for Oxygen Reduction Reaction. *Chem. Commun.* **2013**, *49*, 10112–10114

(5) Lukatskaya, M. R.; Mashtalir, O.; Ren, C. E.; Dall'Agnese, Y.; Rozier, P.; Taberna, P. L.; Naguib, M.; Simon, P.; Barsoum, M. W.; Gogotsi, Y. Cation Intercalation and High Volumetric Capacitance of Two-Dimensional Titanium Carbide. *Science* **2013**, *341*, 1502–1505

(6) Naguib, M.; Mochalin, V. N.; Barsoum, M. W.; Gogotsi, Y. 25th Anniversary Article: MXenes: A New Family of Two-Dimensional Materials. *Adv. Mater.* **2014**, *26*, 992–1005

(7) Naguib, M.; Kurtoglu, M.; Presser, V.; Lu, J.; Niu, J.; Heon, M.; Hultman, L.; Gogotsi, Y.; Barsoum, M. W. Two-Dimensional Nanocrystals Produced by Exfoliation of Ti_3AlC_2. *Adv. Mater.* **2011**, *23*, 4248–4253

(8) Khazaei, M.; Arai, M.; Sasaki, T.; Chung, C.-Y.; Venkataramanan, N. S.; Estili, M.; Sakka, Y.; Kawazoe, Y. Novel Electronic and Magnetic Properties of Two-Dimensional Transition Metal Carbides and Nitrides. *Adv. Funct. Mater.* **2013**, *23*, 2185–2192

(9) Xie, Y.; Kent, P. R. C. Hybrid Density Functional Study of Structural and Electronic Properties of Functionalized $Ti_{n+1}X_n$ (X=C,N) Monolayers. *Phys. Rev. B* **2013**, *87*, 235441

(10) Khazaei, M.; Arai, M.; Sasaki, T.; Estili, M.; Sakka, Y. Two-Dimensional Molybdenum Carbides: Potential Thermoelectric Materials of the MXene Family. *Phys. Chem. Chem. Phys.* **2014**, *16*, 7841–7849

(11) Ando, Y.; Watanabe, S. First-Principles Study of Metal-Insulator Control by Ion Adsorption on Ti_2C MXene Dioxide Monolayers. *Appl. Phys. Express* **2016**, *9*, 015001

(12) Lai, S.; Jeon, J.; Jang, S. K.; Xu, J.; Choi, Y. J.; Park, J.-H.; Hwang, E.; Lee, S. Surface Group Modification and Carrier Transport Properties of Layered Transition Metal Carbides (Ti_2CT_x, T: -OH, -F and -O). *Nanoscale* **2015**, *7*, 19390–19396

(13) Kresse, G.; Furthmüller, J. Efficient Iterative Schemes for Ab Initio Total-Energy Calculations Using a Plane-Wave Basis Set. *Phys. Rev. B* **1996**, *54*, 11169–11186

(14) Perdew, J. P.; Burke, K.; Ernzerhof, M. Generalized Gradient Approximation Made Simple. *Phys. Rev. Lett.* **1996**, *77*, 3865–3868

(15) Blöchl, P. E.; Jepsen, O.; Andersen, O. K. Improved Tetrahedron Method for Brillouin-Zone Integrations. *Phys. Rev. B* **1994**, *49*, 16223–16233

(16) Allen, P. B.; Pickett, W. E.; Krakauer, H. Anisotropic Normal-State Transport Properties Predicted and Analyzed for High-T_c Oxide Superconductors. *Phys. Rev. B* **1988**, *37*, 7482–7490

(17) Schulz, W. W.; Allen, P. B.; Trivedi, N. Hall Coefficient of Cubic Metals. *Phys. Rev. B* **1992**, *45*, 10886–10890

(18) Chaput, L.; Pécheur, P.; Tobola, J.; Scherrer, H. Transport in Doped Skutterudites: Ab Initio Electronic Structure Calculations. *Phys. Rev. B* **2005**, *72*, 085126

(19) Madsen, G. K. H.; Singh, D. J. BoltzTraP. A Code for Calculating Band-Structure Dependent Quantities. *Comput. Phys. Commun.* **2006**, *175*, 67–71

(20) Alfè, D. PHON: A Program to Calculate Phonons Using the Small Displacement Method. *Comput. Phys. Commun.* **2009**, *180*, 2622–2633

(21) Cochran, W.; Cowley, R. A. Dielectric Constants and Lattice Vibrations. *J. Phys. Chem. Solids* **1962**, *23*, 447–450

(22) Baroni, S.; Giannozzi, P.; Testa, A. Green's-Function Approach to Linear Response in Solids. *Phys. Rev. Lett.* **1987**, *58*, 1861–1864

(23) Esfarjani, K.; Stokes, H. T. Method to Extract Anharmonic Force Constants from First Principles Calculations. *Phys. Rev. B* **2008**, *77*, 144112

(24) Li, W.; Lindsay, L.; Broido, D. A.; Stewart, D. A.; Mingo, N. Thermal Conductivity of Bulk and Nanowire $Mg_2Si_xSn_{1-x}$ Alloys from First Principles. *Phys. Rev. B* **2012**, *86*, 174307

(25) Li, W.; Mingo, N.; Lindsay, L.; Broido, D. A.; Stewart, D. A.; Katcho, N. A. Thermal Conductivity of Diamond Nanowires from First Principles. *Phys. Rev. B* **2012**, *85*, 195436

(26) Li, W.; Carrete, J.; A. Katcho, N.; Mingo, N. ShengBTE: A Solver of the Boltzmann Transport Equation for Phonons. *Comput. Phys. Commun.* **2014**, 1747–1758

(27) Ecsedy, D. J.; Klemens, P. G. Thermal Resistivity of Dielectric Crystals Due to Four-Phonon Processes and Optical Modes. *Phys. Rev. B* **1977**, *15*, 5957–5962

(28) Gan, L.-Y.; Huang, D.; Schwingenschlögl, U. Oxygen Adsorption and Dissociation During the Oxidation of Monolayer Ti_2C. *J. Mater. Chem. A* **2013**, *1*, 13672–13678

(29) May, A. F.; McGuire, M. A.; Singh, D. J.; Ma, J.; Delaire, O.; Huq, A.; Cai, W.; Wang, H. Thermoelectric Transport Properties of $CaMg_2Bi_2$, $EuMg_2Bi_2$, and $YbMg_2Bi_2$. *Phys. Rev. B* **2012**, *85*, 035202

(30) Singh, M. P.; Bhandari, C. M. High-Temperature Thermoelectric Behavior of Lead Telluride. *Pramana* **2004**, *62*, 1309–1317

(31) Ravich, Y. I.; Efimova, B. A.; Smirnov, I. A. *Semiconducting Lead Chalcogenides*; Springer US: Boston, MA, 1970; pp 194–206

(32) Ziman, J. *Electrons and Phonons: The Theory of Transport Phenomena in Solids*; The International Series of Monographs on Physics; Clarendon Press, 1996; pp 288–292

(33) Zha, X.-H.; Huang, Q.; He, J.; He, H.; Zhai, J.; Wu, Y.; Francisco, J. S.; Du, S. The Thermal and Electrical Properties of the Promising Semiconductor MXene Hf_2CO_2. *arXiv:1510.08235* **2015**

(34) Ghosh, S.; Bao, W.; Nika, D. L.; Subrina, S.; Pokatilov, E. P.; Lau, C. N.; Balandin, A. A. Dimensional Crossover of Thermal Transport in Few-Layer Graphene. *Nat. Mater.* **2010**, *9*, 555–558

(35) Singh, D. J.; Terasaki, I. Thermoelectrics: Nanostructuring and More. *Nat. Mater.* **2008**, *7*, 616–617